ARPN Journal of Engineering and Applied Sciences

www.arpnjournals.com

BRIDGELESS ISOLATED SEPIC PFC FOR EV BATTERY CHARGING USING ANN CONTROLLER

D. Meena[1], V. Padmathilagam[1] and A. Arulvizhi[2]
[1]Department of Electrical Engineering, Annamalai University, Chidambaram, India
[2]Department of Electrical Engineering, CK College of Engineering and Technology, Cuddalore, India
E-Mail: meenadhandapani86@gmail.com

ABSTRACT

The power quality of an Electric Vehicle (EV) battery charger is improved in this work using a bridgeless isolated single ended primary inductance converter (SEPIC). Owing to the excessive amount of conduction losses associated with the conventional Diode Bridge Rectifier (DBR) based Power Factor Correction (PFC) circuit; a Bridgeless circuit model is preferred in this work. The safe functioning of the PFC circuit is further ensured by selecting an isolated topology over a non-isolated converter topology. With the use of an artificial neural network (ANN) controller, the converter's operation is improved in terms of rising time, overshoot, steady state error and settling time. Distortions in the input current are curtailed with the aid of Hysteresis Current Controller (HCC). The entire work of the proposed converter in terms of design equations and several operating modes is detailed elaborately. The input current displays functioning with a unity power factor for the full charging period. The proposed Bridgeless Isolated SEPIC PFC's efficacy in improving the power quality of the EV charger system is determined using simulation results from MATLAB and hardware implementation utilising a DSP30F411 controller.

Keywords: PFC; EV; power quality; bridgeless isolated SEPIC converter; ANN controller; HCC.

1. INTRODUCTION

The ubiquity of fossil fuel-powered vehicles has led to the release of the excessive amount of tailpipe emissions, which contribute to the serious environmental threat of global warming. Therefore, the automotive industry is putting more attention on electrifying the transportation sector to tackle this issue, which has resulted in the development of EVs [1]. The Battery Energy Storage (BES), which is used for powering the EVs, requires the implementation of a suitable power electronic-based coupling circuit for regulating the charging voltage. Furthermore, according to the IEC 61000-3-2 standard, these circuits are effectively maintained the Power Quality of the input power [2]. An input current's Total Harmonic Distortion (THD) must be kept within a predetermined range in addition to preserving a power factor that is close to unity [3]. So, an AC-DC converter with PFC is introduced to achieve the aforementioned conditions.

In order to achieve AC-DC conversion in customary EV battery chargers, a DBR is added to the frontend of the converter circuit. Some of the prominently used PFC circuits comprise a DBR connected in cascade to a Boost converter. The extensive use of boost-type PFC modules is due to their promising traits, which include their continuous inductor current along with relatively easier control and simple structure. On the flip side, an efficiency of the boost converter downgrades with an increase in its duty cycle. Moreover, owing to the non-linear behaviour of the DBR, a considerable amount of distortions arise on the side of the input supply [4-6]. A substantial amount of conduction losses in a PFC circuit is caused due to a presence of a bridge rectifier, so to overcome this limitation bridgeless (BL) PFC circuits came in existence by excluding the input bridge rectifier. The bridgeless PFC circuits have better efficiency and minimized conduction loss owing to the absence of the conduction diodes [7-9]. The BL-Boost PFC [10] comes with the benefits of continuous input current, unity power factor, lower THD and simple topology. The higher amount of inrush current and peak input voltage present some restrictions, nevertheless, just as its DBR counterpart. Other BL PFC circuits that are offered include BL-Buck PFC [11], BL-Buck Boost PFC [12], BL-Cuk PFC [13] and BL-SEPIC PFC [14, 15]. Among these aforementioned BL PFC topologies, the most popular topology used for EV application is BL-SEPIC converter due to its minimum conduction loss, but on the flip side, it is a non-isolated converter. By choosing a BL Isolated PFC converter over a BL Non-isolated PFC converter since the former isolates the output from problematic input voltage, the safe operation of the circuit is ensured. By using a suitable controller technique, the operation of the BL Isolated PFC converter is further optimised since it significantly reduces the rise time, settling time and steady state error of a converter's dynamic performance indices. PI controller is an appealing controller technology with the capacity to include many control algorithms that is reliable, simple and flexible under a variety of operating settings. It is however less efficient in tackling instantaneous or incessant disruptions during the system operation. Moreover, it is ineffectual in the case of non-linear operating conditions, due to increased oscillations, peak overshoot issues and delayed dynamic response. The Fuzzy Logic Controller (FLC) is another prominently used controller technique, which is efficient at handling non-linearity issues, unlike the PI controller. The Fuzzy controller offers excellent dynamic performance with enhanced capability to manage linear and non-linear systems but it has a computationally complex structure [16-18].

VOL. 18, NO. 6, MARCH 2023 ISSN 1819-6608
ARPN Journal of Engineering and Applied Sciences

www.arpnjournals.com

In this work, a BL Isolated SEPIC PFC is presented to improve the performance of an EV battery charger. A significant amount of conduction losses are curtailed effectively with the use of bridgeless circuit topology. In a similar way, the output voltage is protected from the potentially dangerous input voltage when an isolated converter design is used.ANN controller is used to enhance the working of the BL Isolated SEPIC PFC.

2. PROPOSED SYSTEM DESCRIPTION

In this work, a reliable EV charger circuit utilising BL Isolated SEPIC PFC is presented. In different supply voltage cycles, the proposed PFC converter performs independently. By removing the input DBR circuit, it is possible to significantly reduce the conduction losses related to the switching devices. Figure-1 shows the circuitry for the proposed EV charger.

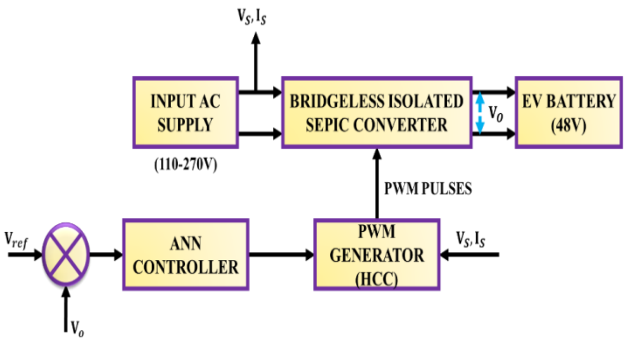

Figure-1. Design for the proposed EV battery charger.

The remarkable control approach of ANN controller is implemented in this work for stabilizing the output obtained from the PFC converter. The desired set reference voltage V_{ref} and the output voltage V_o of the BL Isolated, SEPIC PFC are compared, and an estimated error is subsequently given to an ANN controller. Due to its capacity to provide quick and precise error compensation, an ANN controller was chosen as the main component of the proposed EV charger. The inclusion of non-linear loads affects the input AC supply by triggering an excessive amount of distortions, to improve the power quality of an input side, an HCC is therefore utilised in addition to the ANN controller. The reference current required for the HCC is obtained as output from the ANN controller. The HCC compares the reference current to the input current I_S from the AC supply and performs error compensation. On the basis of the output from the HCC, PWM generator produces pulses for governing the switches of the BL Isolated SEPIC converter. Thus PFC is achieved for the designed on-board EV charger circuit using the BL Isolated SEPIC along with ANN and HCC controller.

3. PROPOSED SYSTEM MODELLING

A. Modelling of Bridgeless Isolated SEPIC Converter

As shown in Figure-2, a bridgeless isolated SEPIC converter is created by combining two isolated SEPIC PFC converter designs. The installation of a common input inductor eliminates the need for input line diodes and the input EMI filter. Following a detailed explanation, the analysis of the BL Isolated SEPIC converter's operation under two distinct operating situations is presented.

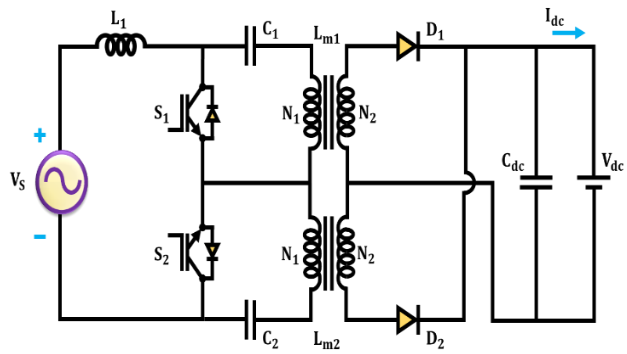

Figure-2. Structure of BL isolated SEPIC topology.

B. Complete Line Voltage Cycle

The BL isolated SEPIC PFC comprises of two switches that function separately in negative and positive half cycle. Throughout the positive half cycle, both the diodeD_1 and switch $S_1$are in ON condition. On the basis of the gating pulses generated by the PWM generator, the switch S_2 remains in OFF condition. As shown in Figure-3, the diode D_2 and switch S_2 both conduct during the negative half cycle, but neither do the diode D_1 and switch S_1 (a-b).

ARPN Journal of Engineering and Applied Sciences

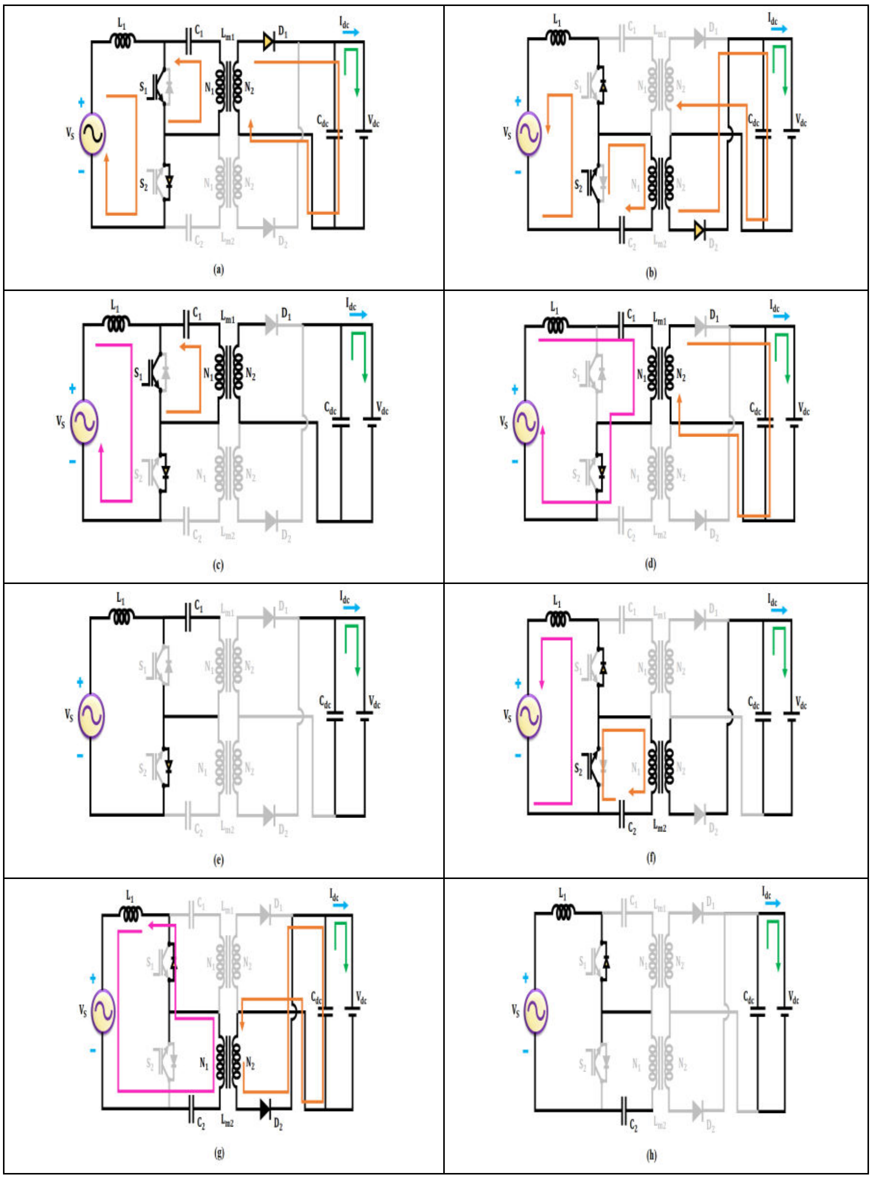

Figure-3. Operating modes of a BL isolated SEPIC converter.

C. Complete Switching Period

According to Figure-3 (c-h), the PFC circuit operates in six different modes during the positive and negative halves of the cycle. The suggested converter's operational waveform for both half cycles is shown in Figure-4.

Mode I $[t_0 - t_1]$.The switchS_1 is in ON condition and a linear surge in the input inductor current is seen with the magnetization of the inductor L_1. The inductor L_{m1} stores the energy discharged from the capacitorC_1 as seen in Figure-3 (c). The current for the battery is supplied from the capacitorC_{dc}.

$$i_{L_i}(t) = I_{L_i}(t_0) + \frac{V_{in}}{L_i}(t - t_0) \quad (1)$$

$$i_{L_{m1}}(t) = I_{L_{m1}}(t_0) + \frac{V_{C1}}{L_{m1}}(t - t_0) \quad (2)$$

On the basis of equation (1) and (2),

$$i_{S_1}(t) = i_{L_i}(t) + i_{L_{m1}}(t) = I_{L_i}(t_0) + I_{L_{m1}}(t_0)\frac{V_{in}}{L_i}(t - t_0) + \frac{V_{C1}}{L_{m1}}(t - t_0) \quad (3)$$

Since$V_{C1} = V_{in}$, equation (3) becomes,

$$\mathrm{i_{S_1}(t) = i_{L_i}(t) + i_{L_{m1}}(t) = I_{L_i}(t_0) + I_{L_{m1}}(t_0)\frac{V_{in}}{L_i//L_{m1}}(t - t_0)} \quad (4)$$

$$i_{D_1} = 0 \quad (5)$$

Where the input inductor current is specified as i_{L_i}, the rated mains voltage is specified as V_{in}, a current through the magnetizing inductance is specified as $i_{L_{m1}}$. The utmost amount of current passing via the switch of the PFC is given as,

$$i_{s1}(t) = I_{L_i}(t_0) + I_{L_{m1}}(t_0) + \frac{V_{in}}{L_i//L_{m1}}DT_S \quad (6)$$

VOL. 18, NO. 6, MARCH 2023 ISSN 1819-6608
ARPN Journal of Engineering and Applied Sciences

www.arpnjournals.com

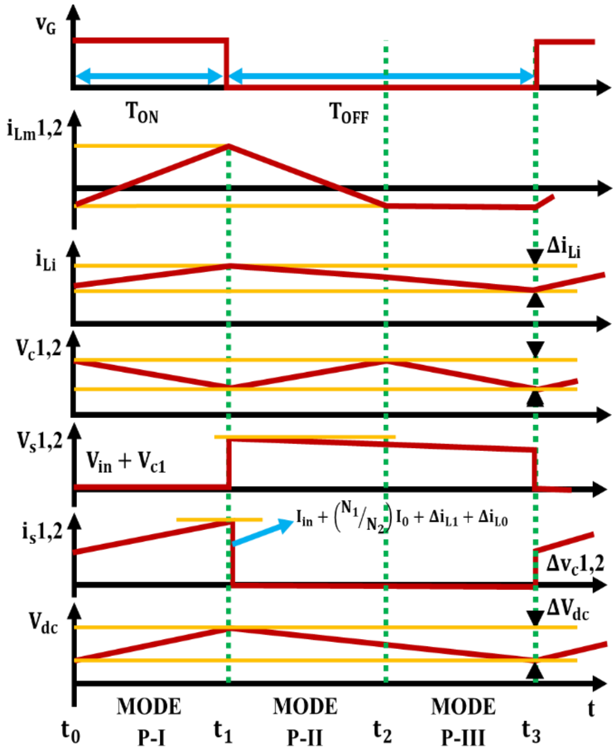

Figure-4. Operating waveform of the BL isolated SEPIC.

Mode II $[t_1 - t_2]$. Unlike mode I, the power switch S_1 is in OFF condition throughout this time period and the diode D_1 conducts due to the flow of currents i_{L_i}andi_{Lm1}. These currents together flow through the diodes D_1 and D_{S_2}. In this mode,

$$V_{in}(t)D + \left(V_{in}(t) - V_{C_1} - nV_{dc}\right)D_1 = 0 \tag{7}$$

$$V_{C1} - nV_{dc} = \frac{D}{D_1}V_{in} \ \ as \ \ D + D_1 \approx D \tag{8}$$

The current through the inductors is given as,

$$I_{Li}(t) = I_{Li}(t_0) + \frac{V_{in}}{L_I}DT_S + \frac{V_{in} - V_{C1} - nV_{dc}}{L_I}(t - t_1) \tag{9}$$

$$= I_{Li}(t_0) + \frac{V_{in}}{L_I}DT_S - \frac{D}{D1}\frac{V_{in}}{L_I}(t - t_1) \tag{10}$$

For$t_1 \leq t \leq DT_S \leq D_1T_S$,

$$\mathrm{I_{Lm1}(t) = I_{Lm1}(t_0) + \frac{V_{in}}{L_{m1}}DT_S + \frac{V_{in} - V_{C1} - nV_{dc}}{L_{m1}}(t - t_1)} \tag{11}$$

$$= I_{Lm1}(t_0) + \frac{V_{in}}{L_{m1}}DT_S - \frac{D}{D1}\frac{V_{in}}{L_{m1}}(t - t_1) \tag{12}$$

$$i_{D_1} = n(i_{Li} + i_{Lm1}) \tag{13}$$

The diode current is derived on the basis of equations (9), (11) and (13)

$$i_{D_1}(t) = n[I_{Li}(t_0) + I_{Lm1}(t_0)] + \frac{V_{in}}{n(L_I//L_{m1})/n^2}(t - t_0) + \frac{V_{in}}{n(L_I//L_{m1})/n^2}(t - t_1) \tag{14}$$

$$\mathrm{= n[I_{Li}(t_0) + I_{Lm1}(t_0)] + \frac{V_{in}}{L_I//L_{m1}}DT_S + \frac{nV_{in}}{L_I//L_{m1}}(t - t_1)} \tag{15}$$

Mode III $[t_1 - t_2]$. The switch S_1 continues to be in OFF condition like in mode II and the inductor current i_{Lm1} is entirely drained. The transfer of energy through the transformer is halted and the diode D_1 also stops conducting. The inductor current is given as,

$$I_{Li}(t) = I_{Li}(t_0) + \frac{V_{in}}{L_i}DT_S + \frac{V_{in} - V_{C1}}{L_i}(t - t_2) \tag{16}$$

$$i_{Lm1}(t) = 0 \tag{17}$$

For$DT_S + D_1T_S = t_2 \leq t \leq T_S$,

$$i_{s1} = 0; i_{D_1} = 0 \tag{18}$$

The similar operational sequence repeats during the negative half cycle. The input inductance is expressed as,

$$L_i = \frac{V_S D}{2f_S \Delta i_i} \tag{19}$$

In this case, the ripple current is provided as f_s and the switching frequency as Δi_i. The magnetising inductance is given as,

$$L_{mc} = \left(\frac{N_1}{N_2}\right)^2 \frac{V_{dc}(1-D)^2}{2Df_S I_{dc}} \tag{20}$$

The capacitance values are expressed as,

$$C_1 = C_2 = \frac{N_2}{N_1}\frac{V_{dc}D}{(\Delta V_C f_S R_{dc})} \tag{21}$$

$$C_{dc} = \frac{I_{dc}}{(2\omega\Delta V_{dc})} \tag{22}$$

The dynamic characteristics of the converter are further improved by the application of ANN controller. With both the PI controller and FLC, the ANN controller's operation is contrasted.

D. ANN for Control of BL Isolated SEPIC PFC

The ANN controller, which replicates the working of a human brain, comprises of several interconnected artificial neurons. Due to its ability to accurately approximate a broad range of nonlinear functions, ANN has recently been used more frequently for the identification and management of nonlinear dynamic systems in power electronics. It is effective in enhancing the stability of the BL Isolated SEPIC PFC by providing a quicker dynamic response. The ANN controller, which has a three-layered architecture, is characterised by numerous attractive qualities such as robustness, quick convergence, tracking ability, low energy consumption, fault tolerance, contextual information processing, adaptability, generalisation ability, learning ability and massive parallelism. Figure-5 represents the BL Isolated SEPIC PFC with ANN controller, while Figure-6 represents the structure of ANN.

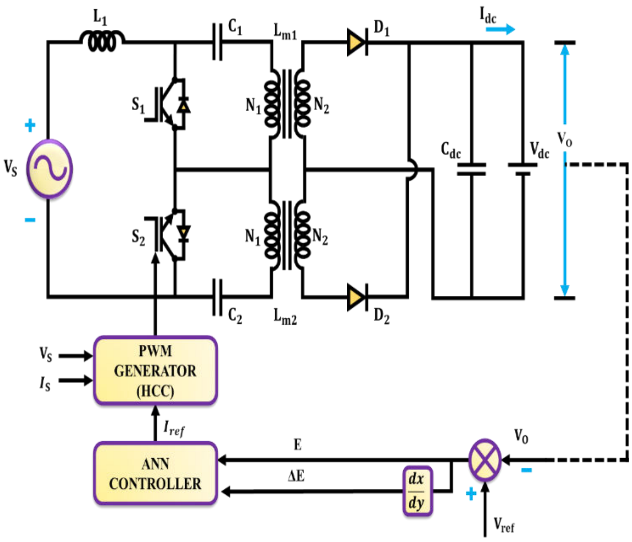

Figure-5. BL Isolated SEPIC with ANN controller.

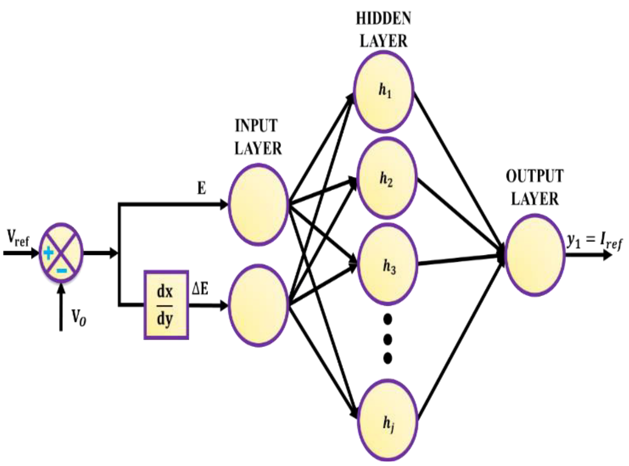

Figure-6. Structure of ANN controller.

By comparing the output voltage obtained from the BL Isolated SEPIC PFC with the required set reference voltage, the value of error is obtained. The obtained value of error in addition to the change in error is given as input to the input layer of the ANN. The obtained error is then processed in the hidden layer on the basis of activation function, bias and weights. Finally, the reference current for the HCC is obtained as output from the output layer. The general mathematical expression used for representing the output obtained from a single neuron is given as,

$$y = Act(b + \sum_{i=1}^{M} e_i \omega_i) \tag{23}$$

Where, the terms M, b, ω_i *and* $Act(.)$represents the number of neurons, bias, weight of every input e_i and the activation function respectively. The sigmoid activation function is given as,

$$Act(.) \equiv f(x) = \frac{1}{1+e^{-x}} \tag{24}$$

The general expression, which is used to represent the output obtained from the ANN layer is given as,

$$y_1 = Act\left(\sum_{j=1}^{J} \omega_{j1} h_j b_1\right) \tag{25}$$

$$h_i = Act(\omega_{mj} e_m + b_j), \forall = \{1, \dots, J\} \tag{26}$$

Where h_i and y_1 are defined, respectively, as the output from output layer and hidden layer. The weights of the output layer and hidden layer is specified as ω_{j1} and ω_{mj} respectively. The total number of hidden layers present is represented as J. The reference current for the HCC is obtained as output from the ANN controller.

E. Modelling of HCC

The HCC compares the source currentI_s to the reference current continuously in order to provide error compensation and aids with the generation of the essential PWM gating pulses for the BL Isolated SEPIC. It is one of the most prominently used instantaneous feedback current control approach owing to its exceptional features such as quick response, excellent accuracy and ease of implementation. In case of variance in both source and load parameters, the HCC displays exceptional performance in terms of error compensation by minimizing the instantaneous errors between the values of control variables and control references. The HCC has a fixed tolerance current band and no operation of switching takes place if the input current is within the band limit. However, the switch S_2 is turned ON if the input current crosses the band limit, which in turn results in the current decay. Similar to this, an input current surge occurs when the input current exceeds the lower band limit, turning ON the switch S_1. Thus the distortions in the input current are minimized using the HCC.

4. RESULTS AND DISCUSSIONS

An on-board EV charger is developed in this work using BL-Isolated SEPIC for achieving effective PFC. The distortions in the input current supply with the addition of a non-linear load is minimized using HCC and a stable output is obtained from the output of the converter using the ANN controller. Using MATLAB simulation, the significance of the proposed on-board EV charger is examined, and the parameter requirements for the design are presented in (Table-1).

VOL. 18, NO. 6, MARCH 2023 ISSN 1819-6608
ARPN Journal of Engineering and Applied Sciences

Table-1. Parameter Requirements.

Parameters	Value
Source voltage	$180V, 220V, 230V$
Source current range for converter	$0-50A$
Output DC voltage	$0-48V$
Battery	$48Ah, 48V$
L_i	$2.38mH$
C_1	$2.36\mu F$
C_2	$2.36\mu F$
C_{dc}	$4700\mu F$
Linear transformer	$1:1\ ratio(230V, 50A, 50Hz)$
L_{m1}, L_{m2}	$315mH$
Switches used	MOSFET
Switching frequency	$100KHz$

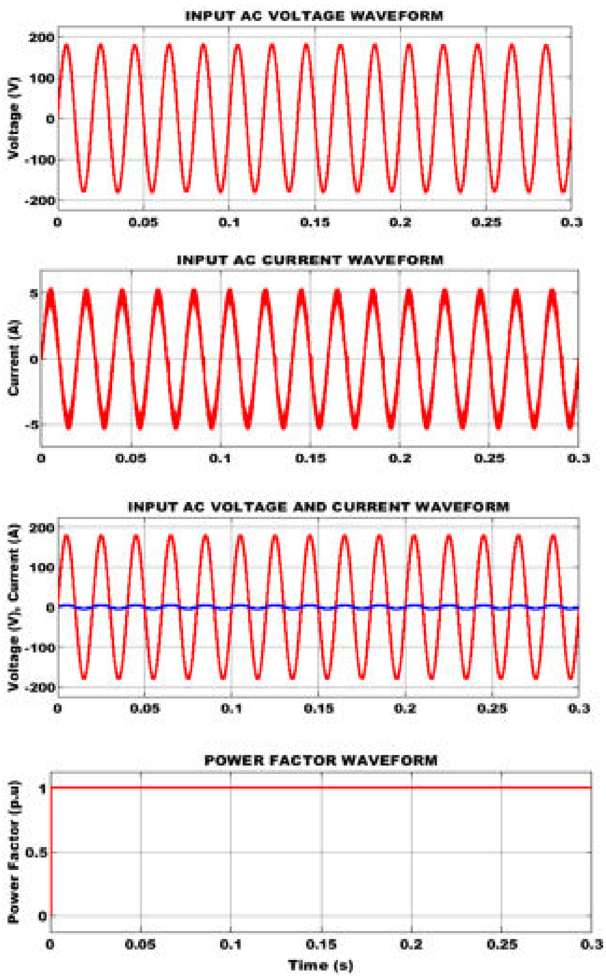

Figure-7. Waveforms for $V_s = 180V$.

Figure-7 displays the obtained waveforms with an input current $I_s = 6A$ and input voltage $V_s = 180V$. An input current and voltage are in phase as mentioned in the above waveform which in turn proves the effective functioning of the proposed approach for improved power factor correction.

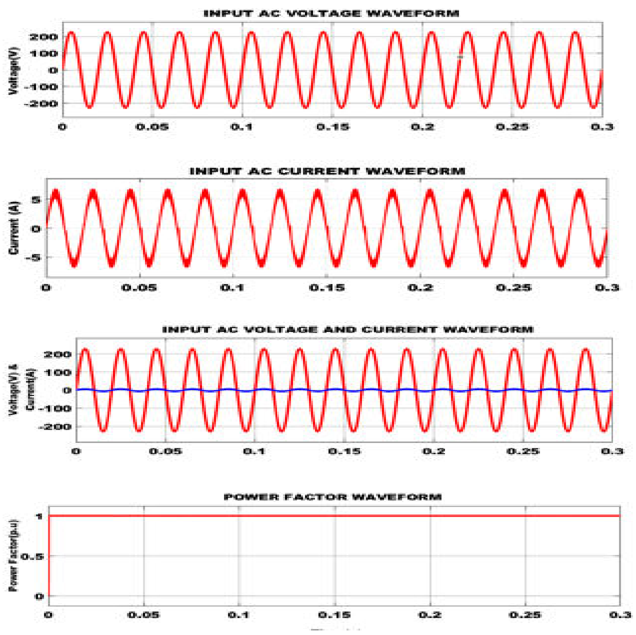

Figure-8. Waveforms for $V_s = 230V$.

Figure-8 indicates the waveforms for the input voltage $V_s = 230V$ in which the corresponding input current is given by $I_s = 7A$. Voltage and current are shown in phase on a third waveform, demonstrating their direct proportionality. This in turn generates improved output for power factor as indicated in the final waveform.

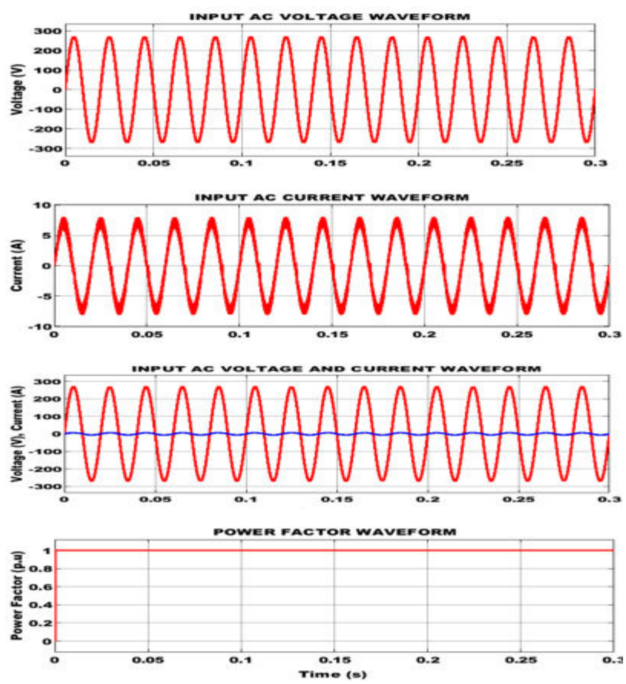

Figure-9. Waveforms for $V_s = 270V$.

The above Figure-9 represents the waveforms for the input voltage $V_s = 270V$ with an input current

VOL. 18, NO. 6, MARCH 2023 ISSN 1819-6608
ARPN Journal of Engineering and Applied Sciences

www.arpnjournals.com

of $I_s = 8A$. Pure resistive elements are present when current and voltage are in phase with one another. This enables improved PFC facilitating enhanced efficiency and the waveform illustrates the power factor mentioned above.

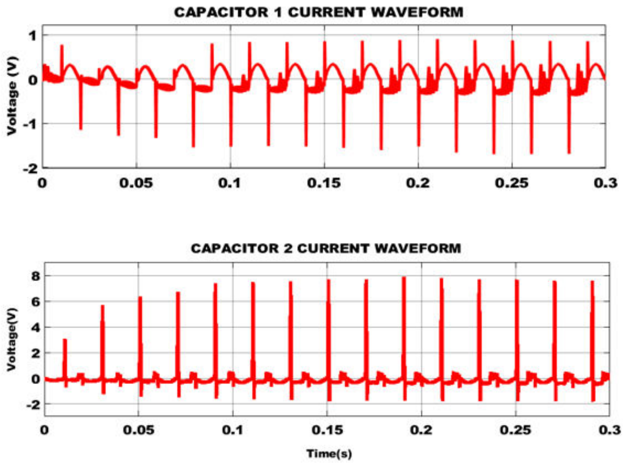

Figure-10. Capacitor current waveforms.

The capacitor current waveforms are shown in Figure-10 in which the output capacitor current waveform exhibits reduced distortions. The output capacitor is connected in parallel minimizing the unwanted voltage drop and performing power factor correction by providing a leading current for compensating the lagging current.

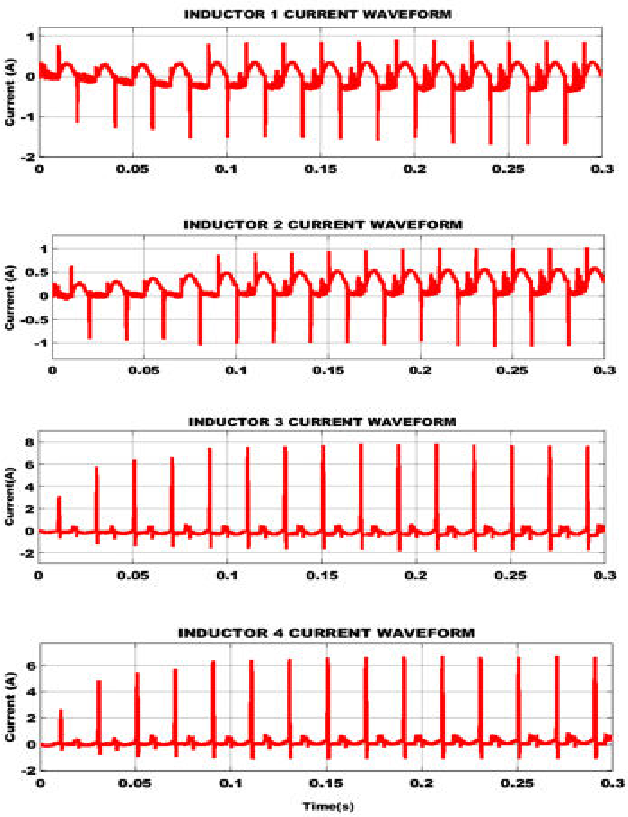

Figure-11. Inductor current waveforms.

Figure-11 denotes the waveforms for the inductor current in which inductors 1 and 2 exhibit current with distortions. Subsequently, inductors 3 and 4 show reduced distortions indicating improved power factor correction.

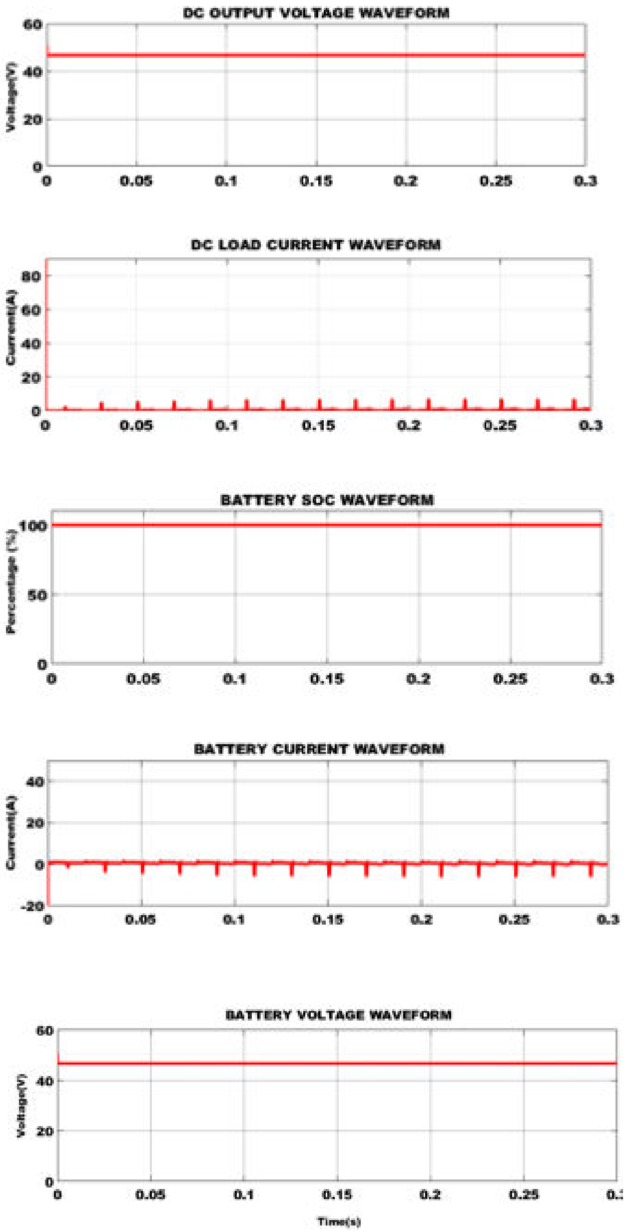

Figure-12. Output waveforms.

Figure-12 represents the output waveforms indicating voltage and current. At varying input voltages of $180V, 230V$ and $270V$, a constant output voltage of $48V$ is attained at the DC link which is further fed to the EV battery. The SOC of the battery is obtained to be 99% with a battery voltage of $48V$. The obtained outputs reveal improved power factor correction in EV battery with enhanced reliability and efficiency.

ARPN Journal of Engineering and Applied Sciences

www.arpnjournals.com

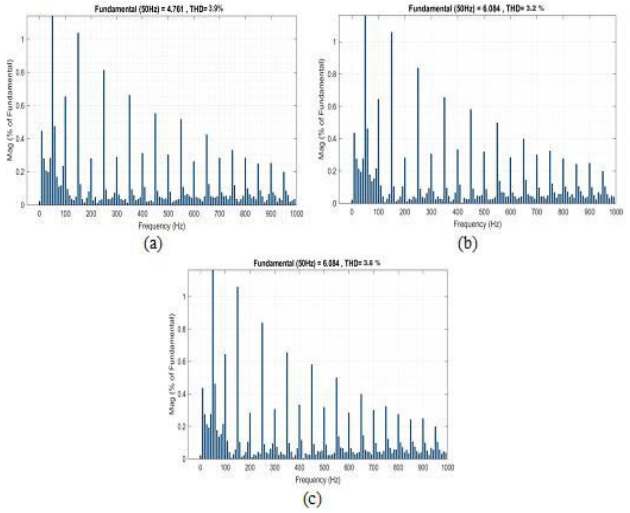

Figure-13. THD outputs for input voltages (a) $180V$ (b) $230V$ (c) $270V$.

Figure-13 represents the obtained THD outputs for different input voltage values like $180V, 230V$ and $270V$. The THD values attained are 3.9% for $180V$, 3.2% for $230V$ and 3.6% for $270V$. With the aid of bridgeless isolated SEPIC-based PFC the harmonics are minimized resulting in reduced THD values.

A. Hardware Results

The hardware validation of the proposed work is carried out by using FPGA which possesses improved performance and configurability as shown in Figure-14. The obtained results indicate the efficacy of the proposed approach and the waveforms are illustrated as follows.

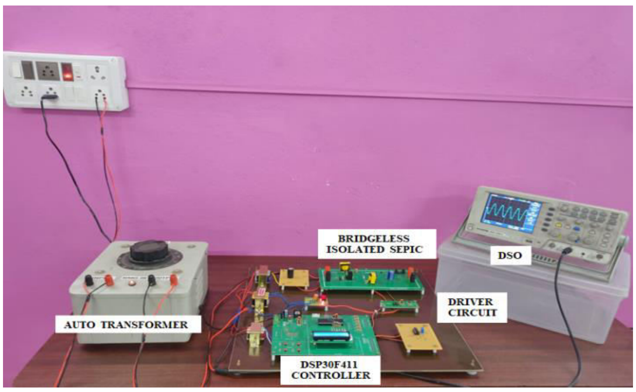

Figure-14. Hardware setup.

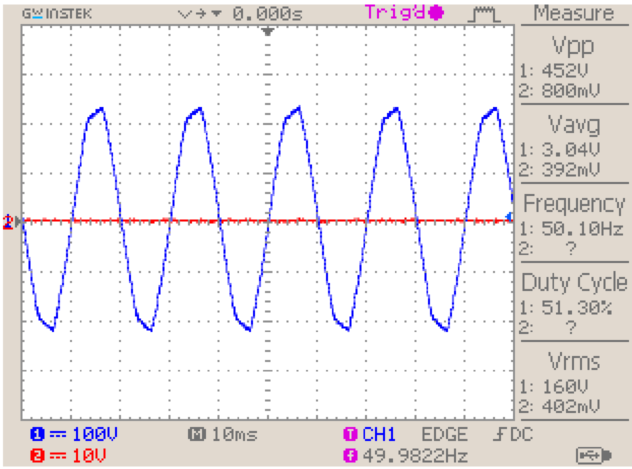

Figure-15. Source voltage waveform.

Figure-15 represents the source voltage waveform considered in the proposed work which is equal to $230V$. Similarly the source current value provided at the input is given by $5A$ as given in Figure-16.

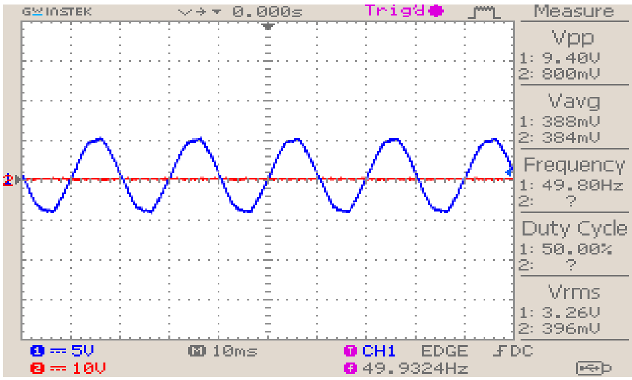

Figure-16. Source current waveform.

According to the aforementioned numbers, the source current and source voltage supplied are in phase with one another and are fed to the bridgeless isolated SEPIC in order to provide increased PFC.

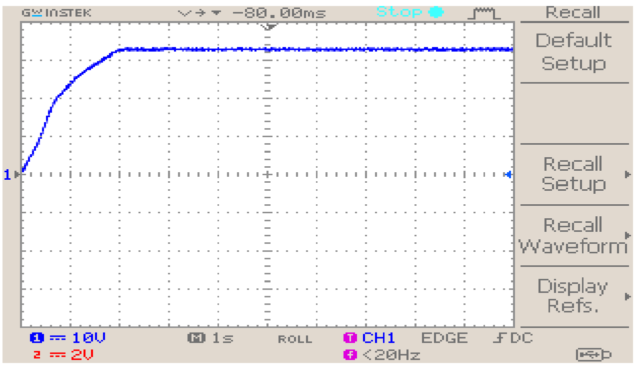

Figure-17. Output voltage waveform for converter.

Figure-17 represents the output obtained from the Bridgeless isolated SEPIC and the waveform clearly indicates that the obtained voltage is free from fluctuations denoting improved PFC. This aids in the generation of unity power factor enabling the controlled operation of the proposed system.

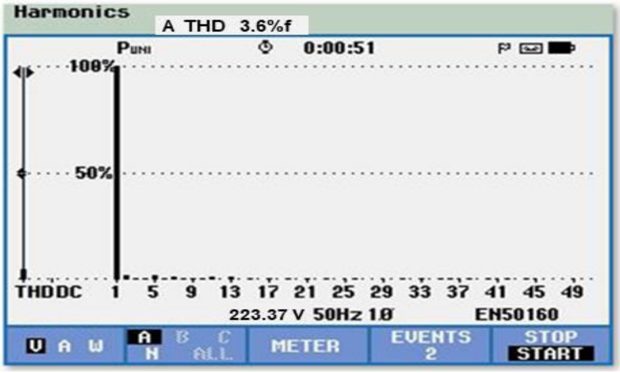

Figure-18. THD output for hardware analysis.

Figure-18 indicates the obtained THD output for the source input of $230V$ with highly reduced harmonics. The THD value is noted to be 3.6% which in turn satisfies the IEEE standard.

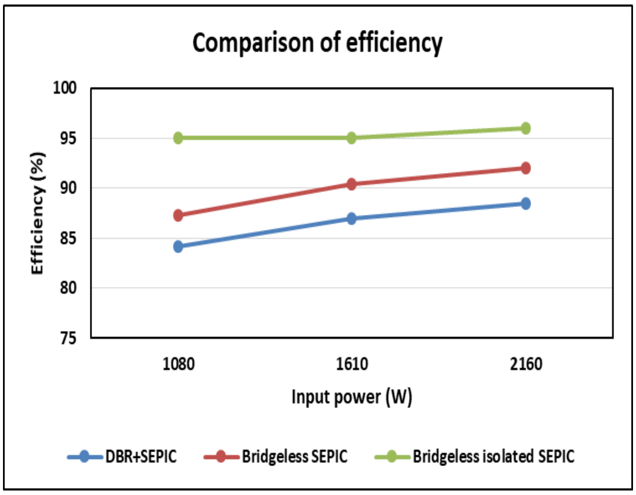

Figure-19. Comparison of efficiency.

Table-2. Power factor comparison.

Converters	Power factor
DBR+SEPIC	0.898
Bridgeless SEPIC	0.988
Bridgeless isolated SEPIC	0.994

Figure-19 shows the comparison of proposed bridgeless isolated SEPIC with DBR-SEPIC and conventional bridgeless SEPIC in terms of efficiency. The proposed converter exhibits enhanced efficiency for varying ranges of input power like $1080W$, $1610W$ and $2160W$ when compared to other existing converters. The overall efficiency of the proposed bridgeless isolated SEPIC is obtained as 95.6%. (Table-2) represents the obtained values of power factor for the proposed converter and other existing converters.

5. CONCLUSIONS

In this paper, a robust on-board EV charger circuit is presented to maintain a unity power factor while also ensuring that the input power quality indices satisfy the required IEC 61000-3-2 standard. A proposed design includes a BL Isolated SEPIC, which comes with the benefit of minimized conduction losses due to the absence of DBR at the input side. The adoption of an isolated circuit topology design ensures that the output is safe from abrupt variations in the input. The addition of a common input inductor greatly lowers the price and size of the charger. The voltage and current distortions at the input side is minimized using ANN and HCC respectively. The ANN controller provides quick and accurate responses even in non-linear operating conditions. On the basis of the hardware implementation and simulation results obtained from MATLAB, an effectiveness of the entire on-board charger design is determined. From the obtained results, it is confirmed that the BL Isolated SEPIC works with a phenomenal efficiency of 95.6% in addition to delivering a reduced THD value.

REFERENCES

[1] M. Ehsani, K. V. Singh, H. O. Bansal and R. T. Mehrjardi. 2021. State of the Art and Trends in Electric and Hybrid Electric Vehicles. in Proceedings of the IEEE. 109(6): 967-984.

[2] B. Singh and R. Kushwaha. 2020. A PFC Based EV Battery Charger Using a Bridgeless Isolated SEPIC Converter. in IEEE Transactions on Industry Applications. 56(1): 477-487.

[3] R. Kushwaha and B. Singh. 2020. Design and Development of Modified BL Luo Converter for PQ Improvement in EV Charger. in IEEE Transactions on Industry Applications. 56(4): 3976-3984.

[4] R. Kushwaha and B. Singh. 2021. Bridgeless Isolated Zeta-Luo Converter-Based EV Charger With PF Preregulation. in IEEE Transactions on Industry Applications. 57(1): 628-636.

[5] S. Meleettil Pisharam and V. Agarwal. 2018. Novel High-Efficiency High Voltage Gain Topologies for AC–DC Conversion with Power Factor Correction for Elevator Systems. in IEEE Transactions on Industry Applications. 54(6): 6234-6246.

[6] J. Itoh and N. Ohtani. 2011. Square-Wave Operation for a Single-Phase-PFC Three-Phase Motor Drive System without a Reactor. in IEEE Transactions on Industry Applications. 47(2): 805-811.

[7] N. Molavi, M. Maghsoudi and H. Farzanehfard. 2021. Quasi-Resonant Bridgeless PFC Converter with Low Input Current THD. in IEEE Transactions on Power Electronics. 36(7): 7965-7972.

[8] H. Wu, Y. Zhang and Y. Jia. 2018. Three-Port Bridgeless PFC-Based Quasi Single-Stage Single-Phase AC–DC Converters for Wide Voltage Range Applications. in IEEE Transactions on Industrial Electronics. 65(7): 5518-5528.

[9] Z. Chen, B. Liu, Y. Yang, P. Davari and H. Wang. 2021. Bridgeless PFC Topology Simplification and Design for Performance Benchmarking. in IEEE Transactions on Power Electronics. 36(5): 5398-5414.

[10] M. -H. Park, J. Baek, Y. Jeong and G. -W. Moon. 2019. An Interleaved Totem-Pole Bridgeless Boost PFC Converter with Soft-Switching Capability Adopting Phase-Shifting Control. in IEEE Transactions on Power Electronics. 34(11): 10610-10618.

[11] X. Lin and F. Wang. 21018. New Bridgeless Buck PFC Converter with Improved Input Current and Power Factor. in IEEE Transactions on Industrial Electronics. 65(10): 7730-7740.

[12] M. Mahmoodsaleh and E. Adib. 2021. Soft-Switching Bridgeless Buck-Boost PFC Converter Using Single Magnetic Core. in IEEE Transactions on Industrial Electronics. 68(7): 5704-5711.

[13] X. Lin, Z. Jin, F. Wang and J. Luo. 2021. A Novel Bridgeless Cuk PFC Converter with Further Reduced Conduction Losses and Simple Circuit Structure. in IEEE Transactions on Industrial Electronics. 68(11): 10699-10708.

[14] H. Ma, Y. Li, J. -S. Lai, C. Zheng and J. Xu. 2018. An Improved Bridgeless SEPIC Converter without Circulating Losses and Input-Voltage Sensing. in IEEE Journal of Emerging and Selected Topics in Power Electronics. 6(3): 1447-1455.

[15] R. Kushwaha, B. Singh and V. Khadkikar, "An Isolated Bridgeless Cuk–SEPIC Converter-Fed Electric Vehicle Charger," in IEEE Transactions on Industry Applications, vol. 58, no. 2, pp. 2512-2526, March-April 2022.

[16] K. Y. Ahmed, N. Z. Bin Yahaya, V. S. Asirvadam, N. Saad, R. Kannan and O. Ibrahim. 2018. Development of Power Electronic Distribution Transformer Based on Adaptive PI Controller. in IEEE Access. 6: 44970-44980.

[17] K. K. Siu, Y. He, C. N. M. Ho, H. S. Chung and R. T. Li. 2019. Advanced Digital Controller for Improving Input Current Quality of Integrated Active Virtual Ground-Bridgeless PFC. in IEEE Transactions on Power Electronics. 34(4): 3921-3936.

[18] M. S. Ali, L. Wang, H. Alquhayz, O. U. Rehman and G. Chen. 2021. Performance Improvement of Three-Phase Boost Power Factor Correction Rectifier through Combined Parameters Optimization of Proportional-Integral and Repetitive Controller. in IEEE Access. 9: 58893-58909.